Transaction B: Mechanical Engineering
Vol. 16, No. 1, pp. 53–63

SCIENTIA IRANICA

Simulation of a Density Current Turbulent Flow Employing Different RANS Models: A Comparison Study

A. Mehdizadeh[1] **and B. Firoozabadi**[1,*]

Abstract. *The accuracy of Reynolds Averaged Navier-Stokes (RANS) turbulence models to predict the behavior of 2-D density currents has been examined. In this work, a steady density current is simulated by the $k-\varepsilon$, $k-\varepsilon$ RNG, two-layer $k-\varepsilon$ and modified $\overline{\nu^2}-f$ model, all of which are compared with the experimental data. Density currents, with a uniform velocity and concentration, enter a channel via a sluice gate into a lighter ambient fluid and move forward down-slope. The eddy-viscosity concept cannot accurately simulate this flow because of two stress production structures found within it. Results show that all isotropic models have a weak outcome on this current, but by improving the ability of the models, the results will improve.*

Keywords: *Density current; Turbulence models; $k-\varepsilon$ RNG; Two-layer $k-\varepsilon$; Modified $\overline{\nu^2}-f$.*

INTRODUCTION

Density current is formed when a heavier fluid than the ambient flows down an inclined bed. These flows, which are common phenomena in nature, can be formed by salinity, temperature inhomogeneities, or suspended particles of silt and clay. These currents are often observed in oceans and large lakes, powder snow avalanches in mountainous areas and pyroclastic flows in volcanic zones. In reservoirs and lakes, density currents are important in managing siltation and water quality.

Previous laboratory experiments of density currents include those performed by Ellison and Turner [1], Rad [2], Alavian [3], Parker et al. [4], Garcia [5], Altinakar et al. [6] and Lee and Yu [7].

In numerical studies, the vertical structure model uses Reynolds equations in order to obtain the flow variables that are non-uniform over the depth. A turbulence closure is required to estimate the Reynolds stresses. Stacey and Bowen [8,9] calculated the vertical distribution of the velocity and concentration profiles of one-dimensional currents and employed a mixing length model for the turbulence closure. Eidsvik and Brrs [10] applied the $k-\varepsilon$ turbulence model and investigated the possibility of self-acceleration of the currents. The vertical structure of density currents has also been studied by Brrs and Eidsvik [11] using the Reynolds stress model. The $k-\varepsilon$ model, which is very popular, has been applied to density currents plunging into reservoirs by Farrell and Stefan [12], Kupusovic [13] and Bournet et al. [14]. Density currents that occur in sedimentation tanks have been simulated by the $k-\varepsilon$ turbulence model in Lyn et al. [15] and Lakehal et al. [16]. Using the low Reynolds number turbulent model, $k-\varepsilon$ (Launder-Sharma turbulence model), Firoozabadi et al. [17] studied the structure of this current.

The $k-\varepsilon$ model has some weaknesses, which cannot accurately simulate behavior near the wall (e.g. over-prediction of eddy viscosity near the wall or inability to simulate anisotropy effects near the wall).

Yakhot and Orszag [18] introduced the Renormalization Group (RNG) model. In the latest version of the RNG k-epsilon model, an additional term has been added in the epsilon equation [19]. According to Pope [20], the additional term in the epsilon equation is an ad hoc model, not derived from the RNG theory. The additional term accounts for the turbulent to mean-strain time scale ratio through the modification of the production coefficient. The term changes dynamically with the rate of the turbulence strain and it is largely responsible for the difference in the performance

1. *Department of Mechanical Engineering, Sharif University of Technology, P.O. Box 11155-956, Tehran, Iran.*
*. *Corresponding author. E-mail: firoozabadi@sharif.edu*

Received 24 August 2006; received in revised form 21 January 2007; accepted 22 April 2007

of the standard and RNG models. In consequence of this operation, the turbulent diffusivity decreases significantly in high shear stress areas, yielding a more realistic behavior of flow.

A compromise between the assertions of a universal wall layer, as made by wall function methods, and a full simulation of the wall adjacent region, is to formulate a simplified model for that layer and patch it onto the full $k-\varepsilon$ model. The full model is solved in the outer region. The $k-l$ formulation has been used to this end, in an approach called the "two layer $k-\varepsilon$ model" [21]. Rodi [22] examined this model on the backward step and his results showed that this model had better results than the $k-\varepsilon$ model, especially in the near wall region. Using the same model combination, Cho et al. [23] performed promising calculations of the two-dimensional unsteady flow field in a linear turbine cascade, including transition on the blade surfaces.

In the last few years, the $\overline{\nu^2}-f$ turbulence model, originally suggested by Durbin [24], has become increasingly popular, due to its ability to correctly account for near-wall damping without using the so-called damping functions. The $\overline{\nu^2}-f$ model in many fluid flows, where complex flow features are present, has shown to be superior to the other RANS methods. For example, Parneix et al. [25] successfully computed the strongly three-dimensional flow around a wall-mounted appendage. Using the $\overline{\nu^2}-f$ model, Hermanson et al. [26] obtained improvements in the prediction of heat transfer rates, as compared to $k-\varepsilon$ computations for a stator vane flow. Similar results were also found in Sveningsson [27]. Another class of flows, where the $\overline{\nu^2}-f$ model seems to work well, is separated flows. Cokljat et al. [28] computed a set of recirculation flows and found that the $\overline{\nu^2}-f$ model in many cases outperformed the two-equation approaches. The same trend was seen in Iaccarino [29], where the flow in an asymmetric diffuser was computed using the $\overline{\nu^2}-f$ model and the Launder-Sharma low-Reynolds number $k-\varepsilon$ model. The separation bubble characteristic of this flow was fairly accurate when predicted with the $\overline{\nu^2}-f$ model, whereas the $k-\varepsilon$ model produced no recirculation at all. Due to the somewhat unstable formulation of the wall boundary condition of relaxation parameter, f, in the original formulation of the $\overline{\nu^2}-f$ model, Lien and Kalitzin [30] slightly redefined f, in order to have a numerically more attractive boundary condition. Due to the improved numerical properties of the redefined model, it has become more popular than the original, which in most cases, required a coupled solution procedure (e.g. [27]). In a recent study of Sveningsson [31], the behavior of two versions of the $\overline{\nu^2}-f$ model is compared, in an attempt to investigate in which aspects they differ and, also, to improve the overall understanding of $\overline{\nu^2}-f$ models performance. In the new study of Heschel et al. [32], 3D wall jets, using different turbulence models, have been compared with each other, using Fluent software. They showed that linear eddy viscosity turbulence models are unable to predict the lateral spreading rate of three dimensional wall jets accurately. If Reynolds stress models are used, it can also be derived that the computed results are very sensitive to the chosen pressure strain models. However, they showed that the $\overline{\nu^2}-f$ model has very good agreement with DNS data.

In this study, a density current was simulated by the $k-\varepsilon$, $k-\varepsilon$ RNG, two-layer $k-\varepsilon$ and modified $\overline{\nu^2}-f$ turbulence models, all of which were compared with experimental data.

MATHEMATICAL MODELING

Governing Equations

Figure 1 shows the schematic sketch of the density current. The salt solution is used as the dense layer and its concentration is so small that a Boussinesq approximation can be used. With this assumption, the effects of the density difference are neglected in the inertial term, but included in the buoyancy force term. However, the governing equations of this current are:

$$\frac{\partial u}{\partial x}+\frac{\partial \nu}{\partial y}=0, \tag{1}$$

$$u\frac{\partial u}{\partial x}+\nu\frac{\partial u}{\partial y}=-\left(\frac{1}{\rho}\right)\frac{\partial P}{\partial x}+g'\sin\theta + \frac{\partial}{\partial y}\left[(\upsilon+\upsilon_t)\frac{\partial}{\partial y}\right], \tag{2}$$

$$u\frac{\partial \nu}{\partial x}+\nu\frac{\partial \nu}{\partial y}=-\left(\frac{1}{\rho}\right)\frac{\partial P}{\partial y}-g'\cos\theta + \frac{\partial}{\partial y}\left[(\upsilon+\upsilon_t)\frac{\partial \nu}{\partial y}\right], \tag{3}$$

$$u\frac{\partial C}{\partial x}+\nu\frac{\partial C}{\partial y}=\frac{\partial}{\partial y}\left[(\lambda+\xi_s)\frac{\partial C}{\partial y}\right], \tag{4}$$

where these equations are continuity, momentums and mass balance and u and ν are streamwise and normal

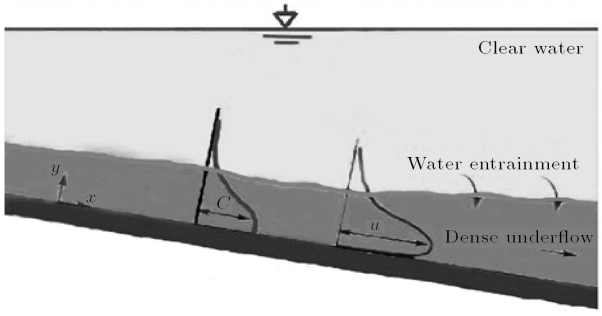

Figure 1. The schematic sketch of the density current.

velocity in x and y directions. C is the concentration of the salt solution, defined as $C = (\rho - \rho_w)/(\rho_s - \rho_w)$ and ρ is the density of the salt-water solution. ρ_s and ρ_w are the salt and water densities. υ and λ are the viscosity and diffusivity of the mixture, respectively. In the momentum equation, g' is the reduced gravitational acceleration, which is defined as:

$$g' = g\frac{\rho - \rho_w}{\rho_w}. \tag{5}$$

In the mass balance equation (concentration equation), ζ_s is the turbulence diffusivity. By using the turbulent Schmidt number, Sc, and turbulence eddy viscosity, υ_t, the eddy diffusivity is defined by:

$$\zeta_s = \frac{\upsilon_t}{\mathrm{Sc}}. \tag{6}$$

While the Schmidt number, similar to the Prandtl number, is predictable to be affected by the buoyancy, there is assumed to be unity here [15].

Turbulence Modeling

When the dense fluid enters the channel and moves forward under the surrounding water, it behaves like a wall jet. A characteristic feature of this current is the presence of both a near-wall layer and a free-shear layer; these layers interact with each other and calculation methods must be capable of describing this interaction. In particular, the damping of normal fluctuations, caused by the presence of the wall, extends into the free shear layer, causing the plane wall jet to spread about 30 percent less than the equivalent free jet [33]. Experimental results show that location of the maximum velocity is too close to the wall and the algebraic model (eddy viscosity concept) predicts that the shear stress must be vanished at the location of zero velocity gradients. In contrast, experiments have shown that the locations of zero shear stress and zero velocity gradients do not coincide and this behavior can be simulated only with a full stress-equation model [32,34]. Physical phenomena involved in density currents are substantially different and have been considered as highly challenging test cases for the validation of turbulence models. Since the density current lies on the bed and at a short distance from the bed, the near wall region is very important. Therefore, the near bed behavior has an important effect on the characteristics of this current. In addition, the presence of the density differences increases the complexities, due to the great source term of body forces and entrainment and interaction with the flow and turbulent kinetic energy production terms. Choi and Garcia [35] studied these effects on the characteristics of the $k-\varepsilon$ turbulence model.

A Standard $k-\varepsilon$ Model

Most predictions in industry involve the use of standard or modified versions of the $k-\varepsilon$ turbulence model, available in much existing CFD software. These models have usually been developed, calibrated and validated using flows parallel to the wall. The standard $k-\varepsilon$ model showed poor results in the near wall region [36,37]. Moreover, since density currents become turbulent at low Reynolds numbers (of order 10^3), the $k-\varepsilon$ model, which has been standardized for high Reynolds number and isotropic turbulence flow, cannot simulate the anisotropy and non-homogenous behavior found near the wall [36,38]. In order to integrate k and ε into the wall, it is common practice to introduce low-Reynolds number damping functions. These are tuned to mimic certain near-wall behaviors [37]. However, all these models use a single-point approach that cannot represent the non-local effects of pressure-reflection that occur near solid boundaries [39].

The $k-\varepsilon$ model equations are as follows:

$$u_j\frac{\partial k}{\partial x_j} = \frac{\partial}{\partial x_j}\left((\upsilon + \frac{\upsilon_t}{\sigma_k})\frac{\partial k}{\partial x_j}\right) + p_k - \varepsilon, \tag{7}$$

$$u_j\frac{\partial \varepsilon}{\partial x_j} = \frac{\partial}{\partial x_i}\left[\left(\upsilon + \frac{\upsilon_t}{\sigma_k}\right)\frac{\partial \varepsilon}{\partial x_j}\right] + \frac{C_1 p_k \varepsilon - C_2\varepsilon^2}{k}, \tag{8}$$

where $u_j = (u, \nu, 0)$ is the mean velocity components; k is turbulent kinetic energy; ε is dissipation; μ and μ_t are dynamic and turbulence viscosity, $P_k = \upsilon_t\left[\frac{\partial u_i}{\partial x_j} + \frac{\partial u_j}{\partial x_i}\right]\frac{\partial u_i}{\partial x_j}$ and υ_t is defined as $\upsilon_t = \frac{\mu_t}{\rho}$.

The constants in the standard $k-\varepsilon$ model are:

σ_k	σ_ε	C_μ	C_1	C_2
1.0	1.3	0.09	1.44	1.92

In these equations, eddy-viscosity is defined as: $\upsilon_t = C_\mu\frac{k^2}{\varepsilon}$.

$k-\varepsilon$ RNG Model

Yakhot and Orszag [18] introduced the Renormalization Group (RNG) model. This model is similar to the $k-\varepsilon$ model, but additional terms should be added to the right hand side of Equation 8, so that it is defined as follows:

$$u_j\frac{\partial \varepsilon}{\partial x_j} = \frac{\partial}{\partial x_j}\left[\left(\upsilon + \frac{\upsilon_t}{\sigma_k}\right)\frac{\partial \varepsilon}{\partial x_j}\right] + \frac{C_1 p_k \varepsilon - C_2\varepsilon^2}{k} - \frac{C_\mu\eta^3(1-\eta/\eta_0)}{1+\beta\eta^3}\frac{\varepsilon^2}{k}. \tag{9}$$

In the last term, η is the turbulent time-scale, proportional to the mean flow time-scale. Therefore, this

model can simulate the off-equilibrium effect. η is defined as:

$$\eta = S\frac{k}{\varepsilon},$$

where:

$$S = \sqrt{2S_{ij}S_{ij}},$$

and:

$$S_{ij} = \frac{1}{2}(u_{i,j} + u_{j,i}).$$

The constants in this model are:

σ_k	σ_ε	C_μ	C_1	C_2	η_0	β
0.8	1.15	0.0865	1.45	1.83	4.38	0.015

This additional term, mathematically, causes a smaller estimation of eddy-viscosity than that of the standard $k-\varepsilon$ model and has a better prediction of the mass transfer from the wall.

Two-Layer $k-\varepsilon$ Model

In the two-layer model, developed by Chen and Patel [21], the bulk of the flow is simulated with models employing a length-scale-determining equation, ranging from the $k-\varepsilon$ eddy-viscosity model to Reynolds-stress models, while the viscosity-affected near-wall region is resolved with a simple one-equation model $k-l$ (model) employing a prescribed length-scale distribution. Therefore, for the near-wall region, the eddy-viscosity and dissipation rate are defined as:

$$v_t = C_\mu\sqrt{k}l_\mu, \qquad \varepsilon = \frac{k^{\frac{3}{2}}}{l_\varepsilon},$$

in which l_μ and l_ε are defined as:

$$l_\mu = C_l y\left(1 - \exp\left(-\frac{\mathrm{Re}_y}{A_\mu}\frac{25}{A^+}\right)\right),$$

and:

$$l_\varepsilon = C_l y\left(1 - \exp\left(\frac{\mathrm{Re}_y}{A_\varepsilon}\right)\right).$$

The constants are as follows:

$$C_l = \kappa C_\mu^{-0.75}, \qquad C_\mu = 0.09, \qquad A_\mu = 50.5,$$

$$\mathrm{Re}_y = \frac{k^{0.5}y}{\upsilon}, \qquad A_\varepsilon = 5.08,$$

and:

$$A^+ = 25.$$

And the $k-\varepsilon$ model should be solved far from the wall region. These models $k-\varepsilon$ (and $k-l$) join at the region where the local Reynolds number is $\mathrm{Re}_y = 250$. This model needs a very fine grid near the wall region, therefore, 2 grids are located under the $y^+ = 1$ and 7 grids are located under the $y^+ = 5$.

$\overline{\nu^2} - f$ Model

An attractive alternative to the $k-\varepsilon$ model is the $\overline{\nu^2}-f$ turbulence model [24]. The reason for this is the availability of an additional turbulent velocity scale generic wall normal Reynolds stress component, $\overline{\nu^2}$. Also, the damping functions can be avoided. By considering the exact transport equations for Reynolds stresses in a fully developed channel flow, it can be readily shown that the production of $\overline{u\nu}$ (the only Reynolds stress component that affects the mean flow field) should be proportional to $\overline{\nu^2}$. In two-equation models, the velocity scale (squared) is not explicitly available, but is replaced by the turbulent kinetic energy, k. As k has a different wall distance dependency (y^2), from $\overline{\nu^2}$ (y^4), this model is expected to be inaccurate as the walls are approached. This deficiency can be controlled to some extent by introducing a damping function that improves the wall distance dependency of $\overline{u\nu}$. Durbin [24] showed that, by simply replacing k with $\overline{\nu^2}$ in the definition of the eddy-viscosity, results were substantially improved. Hence, an alternative interpretation, or definition of the damping function, say f_μ, is $\overline{\nu^2} = f_\mu k$. The main problem with a damping function is that this function can be tuned to only a limited number of test cases. In $\overline{\nu^2} - f$ models, on the other hand $\overline{\nu^2}$ is governed by a separate transport equation and, thus, has the potential of being applicable to a wider range of flow situations. In general, $\overline{\nu^2}$ should be regarded as a scale for the velocity component responsible for turbulent transport. It is proportional to k far from solid walls, while, in the near-wall region, it becomes the velocity fluctuation normal to the solid surface, regardless of the orientation of the surface. One important feature of the $\overline{\nu^2}$ equation is its ability to account for non-local effects (e.g. kinematics blocking) by solving an elliptic relaxation equation for f; a parameter closely related to the pressure strain redistribution term. A modified Helmholtz operator introduces ellipticity, which is amenable to numerical computation. It introduces wall effects by a linear equation. This operator generates turbulence profiles that evolve from the near-wall behavior to far from the solid boundaries. Finally, a mathematical constraint has been added to prevent non-realizability of the eddy viscosity, especially in the stagnation region [40].

For an extensive discussion on this subject, see [41]. The model equations are outlined as follows: The $\overline{\nu^2} - f$ model could be thought of as a simplification of a full Second Moment Closure (SMC) model [40]. For instance, the source terms in the f equation represent a return to isotropy and isotropization models for energy redistribution. In this and in other ways, the important effects of the near-wall anisotropy are represented. However, the $\overline{\nu^2} - f$ model has the advantage of solving the mean flow with an eddy

viscosity, which avoids some computational stability problems that have been encountered with the full SMC models. It is a general geometry turbulence model; valid right up to solid walls. It does not need wall functions, whose universality is increasingly being called into question [42].

In the modified $\overline{\nu^2} - f$ turbulence model, the following transport equations must be solved in order to estimate the eddy viscosity:

$$u.\nabla\overline{\nu^2} = \frac{1}{\rho}\nabla.\left[\left(\mu + \frac{\mu_t}{\sigma_k}\right)\nabla\overline{\nu^2}\right] + kf - 6\frac{\varepsilon\overline{\nu^2}}{k}. \quad (10)$$

Furthermore, the elliptic equation below must be solved as the f equation:

$$f - L^2\nabla^2 f = \frac{C_1}{T}\left[\frac{2}{3} - \frac{\overline{\nu^2}}{k}\right] + C_2\frac{P_k}{k} + 5\frac{\overline{\nu^2}}{kT}. \quad (11)$$

In these equations, the production term is $P_k = \upsilon_t\left(\frac{\partial u_i}{\partial x_j} + \frac{\partial u_j}{\partial x_i}\right)\frac{\partial u_i}{\partial x_j}$ and eddy viscosity, υ_t, is defined as $\upsilon_t = C_\mu\overline{v^2}T$, in which $C_\mu = 0.22$. The source term on the right side of the f-equation (Equation 11) is analogous to the IP from the closure model. The constants are $C_2 = 0.3$ and $C_1 = 0.4$. The length scale (L) and time scale (T) in these equations are introduced as:

$$L = C_L\max\left\{L', C_\eta\left(\frac{\nu^3}{\varepsilon}\right)^{1/4}\right\}, \quad (12)$$

$$L' = \min\left\{\left(\frac{k^{3/2}}{\varepsilon}\right), \frac{1}{\sqrt{3}}\frac{k^{3/2}}{C_\mu\overline{\nu^2}\sqrt{2S^2}}\right\}, \quad (13)$$

$$T = \min\left\{T', \frac{0.6}{\sqrt{3}}\frac{k}{C_\mu\overline{\nu^2}\sqrt{2S^2}}\right\}, \quad (14)$$

$$T' = \max\left\{\frac{k}{\varepsilon}, 6\left(\frac{\upsilon}{\varepsilon}\right)^{1/2}\right\}, \quad (15)$$

where $S = S_{ij}S_{ij}$, $S_{ij} = \frac{1}{2}\left(\frac{\partial u_i}{\partial x_j} + \frac{\partial u_j}{\partial x_i}\right)$ and $C_L = 0.2$. The $\overline{\nu^2} - f$ model requires values of k and ε. They are determined by their equations (Equations 7 and 8); the only revision being to replace $C_{\varepsilon 1}$, either by $1.41\left[1 + 0.045\sqrt{k/\overline{\nu^2}}\right]$ or by $1.3 + 0.25/\left[1 + (0.15d/L)^2\right]^4$ [36]. Either of these increases the dissipation near the wall and improves the prediction of k. This model also needs fine grids near the wall region. The first grid in this model was located at the region in which y^+ was less than one.

Test Cases and Boundary Conditions

The computational domain was defined, based on the two-dimensional laboratory experiments of Garcia [5] and Akiyama [43]. It is supposed that the channel in all cases has 6 m length and other variables are related to its experimental model. Since it is well-known that the behavior of density currents is fully 3D, even in relatively-narrow flumes, the issue as to what extent 2-D simulations can capture the main features of the flow is expected to be addressed. The boundary conditions at the inlet are known and similar to the experimental models. The salt-water solution, as a dense fluid with uniform velocity and concentration, enters the channel under the still bodies of water passing through a sluice gate opening and moves along the bed inclined at angle θ. The schematics of the mesh and boundary conditions have been shown in Figure 2. At the out-flow boundary, the stream-wise gradients of all variables are set to zero. It is expected that the modeling of the outlet has only a local effect on the flow field. At the free surface, the rigid-lid approximation is made. Then, the symmetry condition is applied, which includes zero gradients and zero fluxes perpendicular to the boundary. At the bed, velocities and concentration gradients are set to zero, $U_i = 0$; $k = 0$; $\overline{\nu^2} = 0$; $\varepsilon = 2\upsilon k/y^2$; $\tilde{f} = 0$ and for models, such as the $k - \varepsilon$ model, the wall function has been used in the sub-layer region; it means only one grid located below $y^+ = 30$. Also, for $k-\varepsilon$, $k-\varepsilon$ RNG, the two-layer model and the modified $\overline{\nu^2} - f$ equations, at the free surface, no flux conditions are imposed, i.e., $\frac{\partial k}{\partial y} = \frac{\partial \varepsilon}{\partial y} = \frac{\partial \overline{v^2}}{\partial y} = \frac{\partial f}{\partial y} = 0$ and, at the inlet $k_{\text{in}} = (0.1u_{\text{in}})^2$ and $\varepsilon_{\text{in}} = 10k_{\text{in}}^{3/2}/h_{\text{in}}$, in which h_{in} = inlet height, are used [44]. To verify the results of these models, three data sets, such as the height of the body and the non dimensional velocity profiles from different researchers, have been examined.

Solver

Using the pressure correction scheme SIMPLEC and a collocated grid arrangement with the Rhie-Chow [45] interpolation, a finite volume code was developed. The Loda scheme was used to discrete the momentums,

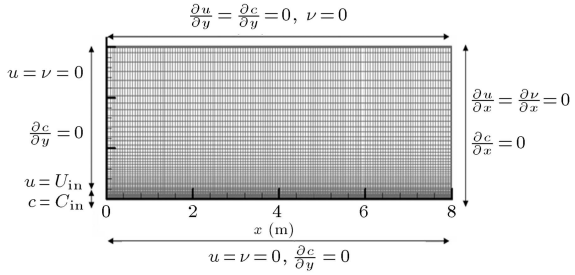

Figure 2. The schematic of mesh and boundary conditions.

turbulence and diffusion equations. Due to the convergence problems, the multi grid method was used to enhance the numerical stability. The equations were solved with a coupled tri-diagonal matrix algorithm (TDMA). All fluid properties were treated as being constant. Convergence of the solution was obtained when the maximum summation of the residuals in all nodes was less than 10^{-3}. The mean flow variables, such as mean flow velocity, are grid independent for all models; it was found that these models were not sensitive about the number of meshes in the x direction. 100 meshes in that direction were enough, but in order to prevent numerical problems, because of the aspect ratio of the grid cells, it was endeavored to reduce the aspect ratio, especially for two-layer and $\overline{\nu^2} - f$ models in the near wall region. So, for unity, 140 meshes were used in an x direction for all models. In the y direction, these models needed different strategies for mesh generation, which has been previously explained.

RESULTS AND DISCUSSION

Figure 3 shows the height of the steady state density current in comparison with the experimental data of Akiyama [43]. In the experimental efforts, it is common to measure the height of this current via its brightness using optical instruments. Therefore, in this work, it was supposed that the height of the current is the location where the concentration is equal to 1% of the inlet concentration (like the boundary layer approach).

It can be seen that all the $k - \varepsilon$ based models have overshot the height of the current. It seems that these models overestimate the eddy viscosity near the wall [39], so the friction coefficient increases, causing the growth of the dense layer to be overshot. On the other hand, at the interface, because of the large diffusion term in the $k - \varepsilon$ model (consequently, in the other approach of the $k - \varepsilon$ model), the dense layer shows very rapid spreading. However, as the ability of the models improves, the height decreases. In the face of the $k-\varepsilon$, $k-\varepsilon$ RNG and two-layer $k-\varepsilon$ model, which cannot simulate anisotropic effects, the $\overline{\nu^2} - f$ model can simulate anisotropic behavior near the bed and free shear layer; therefore, the agreement between predicted and experimental results is very good. Moreover, in this figure, it is seen that, by increasing the inlet Reynolds number, the growth rate of the dense layer decreases. Figure 4 shows the comparison among RANS models to predict the bed skin-friction coefficient. At the inlet section, an internal hydraulic jump probably forms and a large amount of mixing causes entrain of clear water. This figure illustrates that all models come together far from the inlet, but at the inlet section, which has large anisotropic effects, shear rate and mixing, these models estimate different friction coefficients and turbulent kinetic energy. Figure 4 also

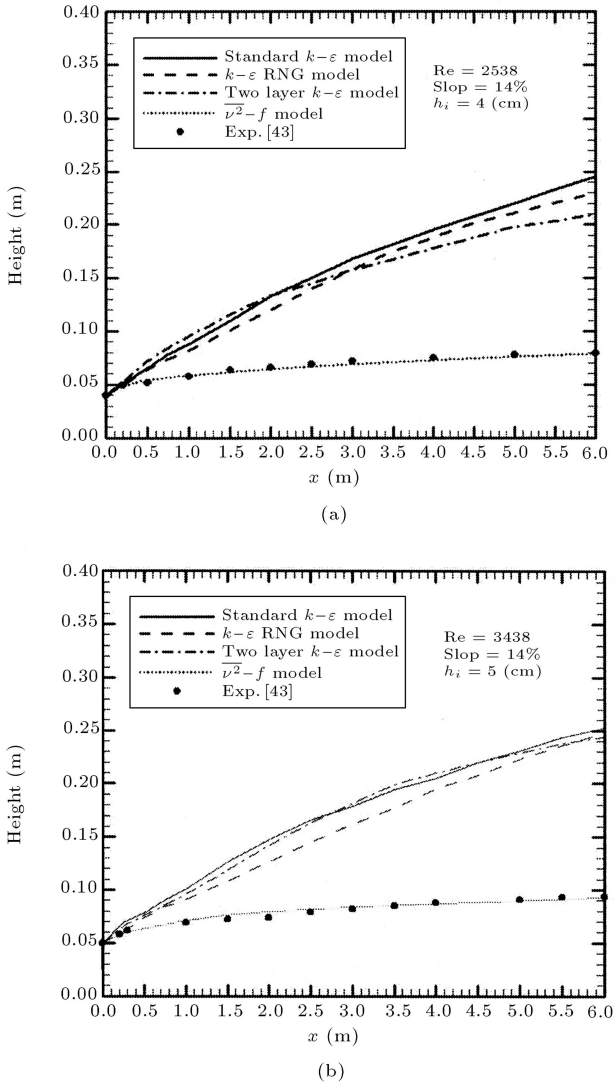

Figure 3. The steady density current height with the RANS models, in comparison with the experimental data (at two different inlets Reynolds number).

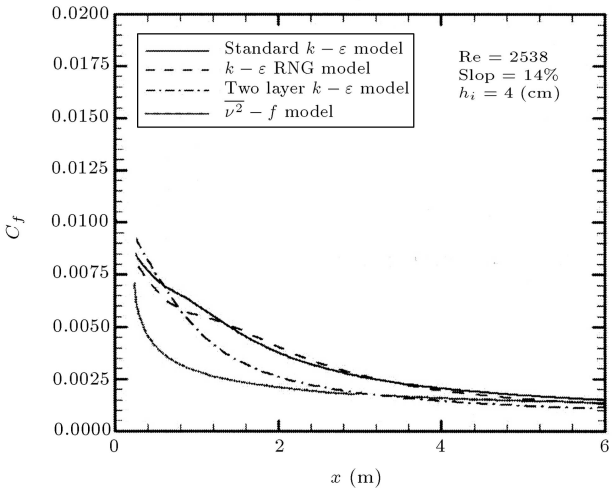

Figure 4. The friction coefficient computed by RANS models.

shows that after a short distance, the density current becomes established; i.e. C_f becomes almost constant and the drag force and buoyancy are balanced with each other. The $k-\varepsilon$ model has over-predicted the turbulent kinetic energy in the shear layer and has caused an increase in the entrainment rate, so the height of the current overshoots. The two-layer model shows a similar weakness, but the $k-\varepsilon$ RNG predicts low turbulent kinetic energy in this region. In Figure 5, velocity vectors and turbulent kinetic energy contours are shown. This figure illustrate that the turbulent kinetic energy in the shear layer has greater effects than the bed friction coefficient on the height of the current. It is remarkable that the height of the body is proportional to the shear layer turbulence intensity and the bed friction coefficient, respectively.

Figure 6 shows the computed vertical structure of the dense underflow, and illustrates that the turbulent kinetic energy in the shear layer develops on an inclined bed. In this figure, the stream-wise velocity is given in a dimensionless form. That is, the vertical axis is non-dimensionalized by the local current thickness, and the horizontal axis is non-dimensionalized by the layer-averaged value. The layer-averaged quantities can be calculated as follows [1]:

$$U = \frac{\int_0^h u dy}{h}, \tag{16}$$

$$C_{av} = \frac{\int_0^h C dy}{h}, \tag{17}$$

where U is layer-averaged velocity of the layer and C_{av} is layer-averaged concentration of the layer.

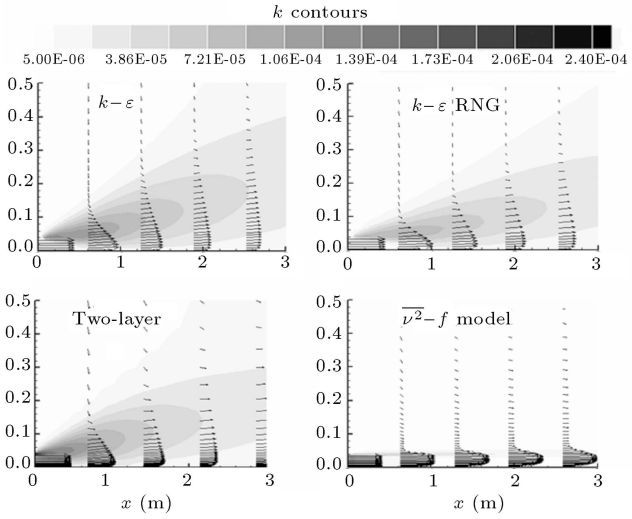

Figure 5. The turbulent kinetic energy contours and velocity profiles computed by RANS models $\mathrm{Re}_i = 2538$, $hi = 4$ (cm).

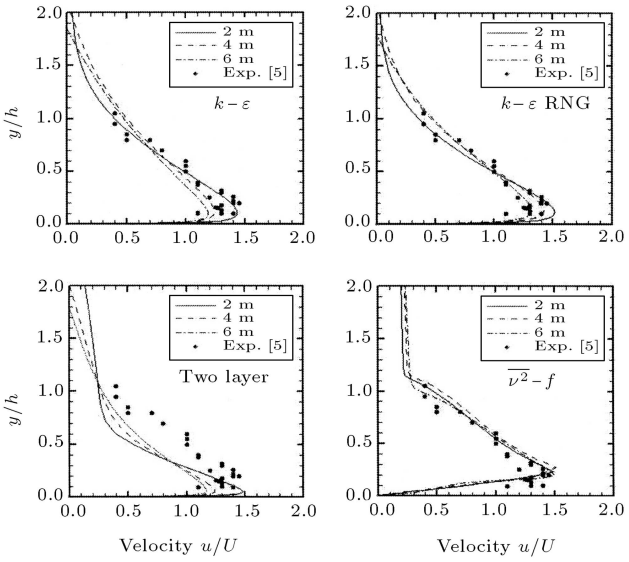

Figure 6. Similarity collapse of vertical structure of dense underflow.

Figure 6 shows the velocity profile at some downstream locations computed with RANS models. It is seen that all of the models are almost fitted with the experimental data (especially $\overline{\nu^2}-f$ model), but according to Figure 3, the $k-\varepsilon$, $k-\varepsilon$ RNG and two-layer $k-\varepsilon$ models have over-estimated in body-height. It seems this point comes from the properties of the dimensionless profile, which has no sense of the body height expansion rate. It can be seen from Figure 6 that the maximum velocity occurs quite close to the channel bottom, particularly in the two-layer model, which used one equation model in this region. Good agreement between computed solutions and experimental results is obtained. Therefore, the $\overline{\nu^2}-f$ model has much better results on this current (both regarding body height and dimensionless velocity profiles).

Entrainment Concept

Due to the presence of shear layer at the interface of the density current and ambient fluid, the interface is disturbed and the surrounding fluid is entrained. Turbulence at this boundary entrains the stationary ambient fluid immediately above it into the layer and dilutes it. The turbulent region grows with distance downstream as the non-turbulent fluid becomes entrained in it. Therefore, a small mean vertical velocity perpendicular to the mean flow is generated when the ambient fluid is initially at rest. Ellison and Turner [1] suggested that the velocity of the inflow into the turbulent region must be proportional to the velocity scale of the layer; the constant of this proportionality is called the entrainment coefficient, E.

If a 2-D flow is considered and, therefore, if the lateral entertainment is neglected, the entrainment

coefficient, E, is defined as:

$$\frac{d(UA)}{dx} = EUb_0, \tag{18}$$

where A is area of cross section of the dense layer; U is layer-averaged velocity; and b_0 is the width of the layer. Entrainment is governed by the bottom slope, friction and mixing at the interface of the dense layer. In this study, the entrainment coefficient is derived by:

$$E = \frac{1}{U}\frac{d}{dx}(Uh), \tag{19}$$

where h is the local height of the density current. The entrainment coefficient of the density current, calculated with RANS models, is shown in Figure 7 along the downstream for $\mathrm{Re_{in}} = 2538$. It can be seen that, due to the higher shear rate, E is maximum at the inlet. Hence, greater turbulent kinetic energy production and larger mixing is generated in this region. Then, E decreases to an almost constant, as the flow becomes established. It can be seen that the model which predicts greater turbulent kinetic energy (Figure 5) in the shear layer region provides the greater entrainment coefficient.

Figures 8 and 9 show the layer-averaged velocity and concentration at the downstream locations computed with RANS models. In Figure 8, it can be seen that the average velocity computed by the $\overline{\nu^2} - f$ model decreases very slowly, but other models predict very rapid decreasing in the averaged velocity. This comes from the fact that the $\overline{\nu^2} - f$ model predicted the growth of the height truly and slowly (Figure 3).

Figure 9 illustrates that the layer-averaged concentration decreases at the downstream and it can be seen that the averaged concentration, velocity and height of current (Figure 3) are linked to each other.

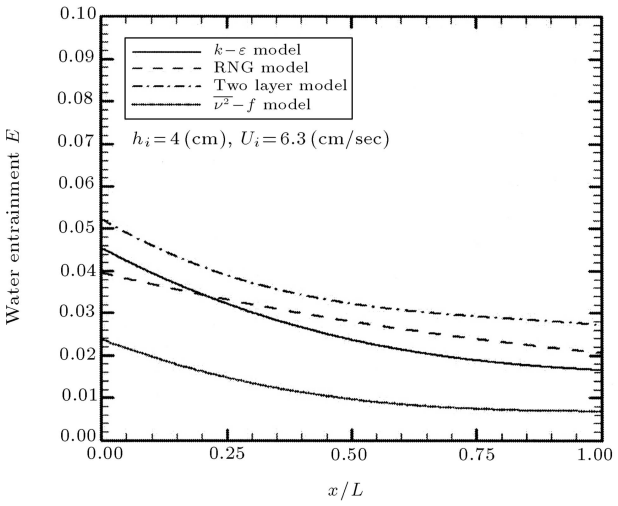

Figure 7. The entrainment coefficient.

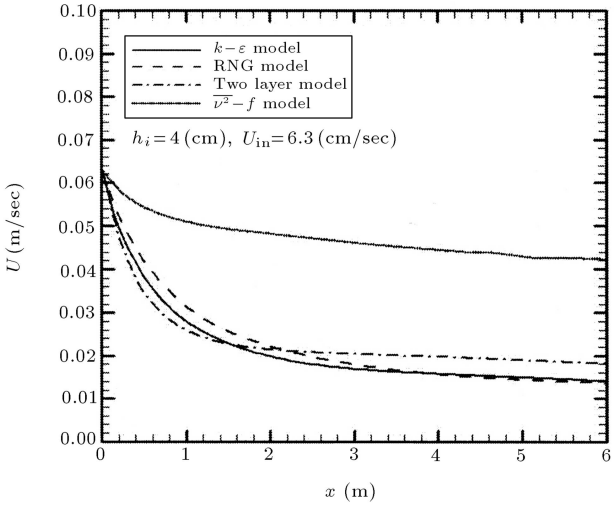

Figure 8. Averaged velocity along the bed (Equation 15).

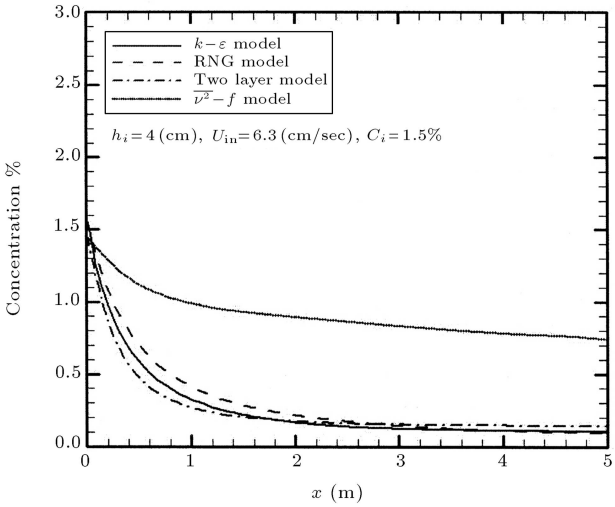

Figure 9. Averaged concentration along the bed (Equation 16).

Moreover, this figure illustrates that the averaged concentration simulated by the two-layer model decreases very rapidly near the inlet section, due to over prediction in mixing intensity and entrainment. It is very attractive that this decreasing rate (Figures 8 and 9) is proportional to the amount of turbulent kinetic energy, which is shown in Figure 5. For example, the $k - \varepsilon$ RNG model, which produces the smaller amount of turbulent kinetic energy near the inlet section, predicts a smaller mixing and slighter decreasing in the averaged concentration compared to that of the $k-\varepsilon$ or the two-layer models in this section.

Comparing RANS Models

According to the solution procedure and mesh generation, it is considered that the $\overline{\nu^2} - f$ model has the best results and can simulate this current very well,

Table 1. Summary results of the RANS models, using a 2000 MHZ Pentium-4 processor.

Models	$k-\varepsilon$	$k-\varepsilon$ **RNG**	**Two Layer**	$\overline{\nu^2}-f$
Iteration	O (1200)	O (1400)	O (1200)	O (3000)
Run Time/Run Time $k-\varepsilon$	1 (3 hr approx.)	1.3 (4 hr approx.)	2.1 (6 hr approx.)	4.5 (13 hr approx.)
Number of Grids	140×54	140×54	140×77	140×66
Wall Function	Used	Used	Not used	Not used
Accuracy in This Case	Function insufficient	Function insufficient	Function poor	Function well

with about a 4.5 times increase in time consumption per iteration, in comparison with the standard $k-\varepsilon$ model. Since the $\overline{\nu^2}-f$ model has two equations more than the $k-\varepsilon$ model, normally, it needs 40% more time to solve these additional equations. On the other hand, these equations impose additional cost because of their computational stability problems, reduction methods for which are required (e.g. multi grid method). Moreover, access to convergence is hard in this model and needs very fine grids near the bed. The two-layer $k-\varepsilon$ model also needs very fine grids near the bed, so the computational cost is more than the $k-\varepsilon$ model. However, its results are not proportional to this increased cost at least in this test-case. The $k-\varepsilon$ RNG model has better results than the $k-\varepsilon$ model. Although its computational cost is almost similar to the standard $k-\varepsilon$ model, its convergence needs more attention. In this study, by considering both computational cost and result accuracy, the $\overline{\nu^2}-f$ model is the best model and completely worthy of use. The $k-\varepsilon$ RNG model, standard $k-\varepsilon$ model and two-layer $k-\varepsilon$ model are known as the next ranks. Using a 2GHz Pentium-IV processor, Table 1 shows a comparison between these 4 models. In this table, it is seen that, in the $\overline{\nu^2}-f$ model, convergence accessibility is difficult and it needs roughly 2.5 times more iterations than the others. Moreover, although the two-layer model is perfect in the sub-layer region, it seems that the shear layer has greater effects on this current than that of the sub-layer region. Also, this model over-estimates the turbulent kinetic energy in the shear layer. On the other hand, since the $\overline{\nu^2}-f$ model uses excellent turbulent time and length-scale in the domain, its prediction is the best among other models, especially in the shear layer and near the wall region. Finally, if one ignores the $\overline{\nu^2}-f$ model, because of its cost and complexity in the convergence and numerical stiffnesses, the $k-\varepsilon$ RNG model will be the second most accurate and efficient turbulence model option to simulate this current.

CONCLUSIONS

Four turbulence models have been applied to simulate the structure of the density current. Momentums, continuity, diffusion equations of the salt-water solution and turbulence equations are solved simultaneously by the SIMPLEC method, without any limitations or simplifications. The computed height of the dense underflow, velocity, concentration and other characteristics were compared with one another and with the experimental data. It was also shown that the density current is very sensitive to the type of turbulence model which simulates it, because of the structure of this current, which is like a wall jet. Moreover, it has been shown that the $\overline{\nu^2}-f$ model has the best result on this current, especially in calculating the shear layer and near the bed characteristics, according to its ability to simulate the anisotropy effects in the domain.

NOMENCLATURE

b_0	width of the layer
$C_\mu, C_{\varepsilon 1}, C_{\varepsilon 2}$	constants in the $k-\varepsilon$ model
C	concentration
ε	energy dissipation rate
E	water entrainment coefficient
f_μ	damping function
f	relaxation variable
g	gravity
g'	reduced gravity
H	water depth
h	density currents height
κ	Von Karman constant
k	turbulent kinetic energy
L	length-scale of turbulence
P_k	production term
Ri	bulk Richardson number
S_{ij}	strain rate tensor
S	$S^2 = S_{ij}S_{ij}$
T	time scale of turbulence
$U = U_{av}$	layer-averaged velocity in the x direction
u^*	shear velocity
u, ν	x and y directions, respectively
$u_i u_j$	Reynolds stresses

$\overline{\nu^2}$	turbulent velocity scale
y	wall normal distance
υ_t	turbulence viscosity
$\sigma_k, \sigma_\varepsilon$	turbulence constants
ρ_w	density of water
ρ_s	density of salt solution
θ	channel slope angle

REFERENCES

1. Ellison, T.H. and Turner, J.S. "Turbulent entrainments in stratified flows", *Journal of Fluid Mech.*, **6**, pp. 423-448 (1959).
2. Rad, M. "The deposition of silt in reservoirs by density current", Ph.D. Thesis, Imperial Coll., London, UK (1976).
3. Alavian, V. "Behavior of density currents on an incline", *J. Hydraulic Eng., ASCE*, **112**(1), pp. 27-42 (1986).
4. Parker, G., Garcia, M., Fukushima, Y. and Yu, W. "Experiments on turbidity currents over an erodible bed", *J. Hydraulic Res.*, **25**(1), pp. 123-147 (1987).
5. Garcia, M. "Hydraulic jumps in sediment-driven bottom current", *J. Hydraulic Eng., ASCE*, **119**(10), pp. 1094-1117 (1993).
6. Altinakar, M.S., Graft, W.H. and Hopfinger, E.J. "Flow structure in turbidity current", *J. Hydraulic Res.*, **34**(5), pp. 713-718 (1996).
7. Lee, H.Y. and Yu, W.S. "Experimental study of reservoir turbidity current", *J. Hydraulic Eng., ASCE*, **123**(6), pp. 520-528 (1997).
8. Stacey, M.W. and Bowen, A.J. "The vertical structure density and turbidity currents: theory and observations", *J. Geophys. Res.*, **93**(C3), pp. 3528-3542 (1988a).
9. Stacey, M.W. and Bowen, A.J. "The vertical structure of turbidity currents and a necessary condition for self-maintenance", *J. Geophys. Res.*, **93**(C3), pp. 3543-3553 (1988b).
10. Eidsvik, K.J. and Brrs, B. "Self-accelerated turbidity current prediction based upon (k-e) turbulence", *Cont. Shelf Res.*, **9**(7), pp. 617-627 (1989).
11. Brrs, B. and Eidsvik, K.J. "Dynamic Reynolds stress modeling of turbidity currents", *J. Geophysics. Res.*, **97**(C6), pp. 9645-9652 (1992).
12. Farrell, G.J. and Stefan, H.G. "Mathematical modeling of plunging reservoir flows", *J. Hydraulic Res.*, **26**(5), pp. 525-537 (1988).
13. Kupusovic, T. "A two dimensional model of turbulent flow applied to density currents', *Proc. Computational Modeling and Experimental Methods in Hydraulics (HYDROCOMP'89), Elsevier Applied Science*, England (1989).
14. Bournet, P.E., Dartus, D., Tassin, B. and Vincon-Leite, B. "Numerical investigation of plunging density current", *J. Hydraulic Eng., ASCE*, **125**(6), pp. 584-594 (1999).
15. Lyn, D.A., Stamou, A.I. and Rodi, W. "Density currents and shear-induced flocculation in sedimentation tanks", *J. Hydraulic Eng., ASCE*, **118**(6), pp. 849-867 (1992).
16. Lakehal, D., Krebs, P., Krijgsman, J. and Rodi, W. "Computing shear flow and sludge blanket in secondary clarifiers", *J. Hydraulic Eng., ASCE*, **125**(3), pp. 253-262 (1999).
17. Firoozabadi, B., Farhanieh, B. and Rad, M. "The propagation of turbulent density currents on sloping bed", *Intl. J. Scientia Iranica*, **8**(2), pp. 223-235 (2001).
18. Yakhot, V. and Orszag, S.A. "Renormalization group analysis of turbulence, I. basic theory", *Journal of Scientific Computation*, **1**, pp. 1-51 (1986).
19. Yakhot, V. and Smith, L.M. "The renormalization group; the epsilon-expansion and derivation of turbulence models", *J. Sci. Comput.*, **7**, pp. 35-48 (1992).
20. Pope, S.B., *Turbulent Flows*, Cambridge Univ. Press (2000).
21. Chen, C.J. and Patel, V.C. "Near-wall turbulence models for complex flows including separation", *AIAA J.*, **26**(6), pp. 641-648 (1988).
22. Rodi, W. "Experimence with two-layer models combining the k-epsilon model with a one-equation model near the wall", *29th Aerospace Science Meeting*, Reno, NE, USA (1991).
23. Cho, N., Liu, X., Rodi, W. and Schonung, B. "Calculation of wake-induced unsteady flow in a turbine cascade", *ASME, J. of Turbomachinery*, **115**(4), pp. 675-686 (1993).
24. Durbin, P. "Near-wall turbulence closure without damping functions", *Theoretical and Computational Fluid Dynamics*, **3**(1), pp. 1-13 (1991).
25. Parneix, S., Durbin, P. and Behnia, M. "Computation of 3-D turbulent boundary layer using the $\overline{\nu^2} - f$ model flow", *Turbulence and Combustion*, **60**(1), pp. 19-46 (1998).
26. Hermanson, K., Kern, S. and Pareneix, S. "Prediction of external heat transfer for turbine vanes and blades with secondary flow fields", *J. of Turbomachinery*, **125**(1), pp. 107-113 (2003).
27. Sveningsson, A. "Analysis of the performance of different $\overline{v^2} - f$ turbulent models in a stator vane passage flow", Licentiae Thesis, Department of Thermo and Fluid Dynamics, Chalmers University of Technology, Gothenburge, Sweden (2003).
28. Cokljat, D., Kim, S., Iaccarino, G. and Durbin, P. "A comparative assessment of the $\overline{v^2} - f$ model for recirculating flows", *41st Aerospace Sciences Meeting and Exhibit*, Reno, Navada (Jan. 6-9, 2003).

29. Iaccarino, G. "Predictions of a turbulent separated flow using commercial CFD codes", *J. of Fluids Engineering, ASME*, **123**(4), pp. 819-828 (2001).

30. Lien, F. and Kalitzin, G. "Computations of transonic flow with the $\overline{v^2} - f$ turbulence model", *International Journal of Heat and Fluid Flow*, **22**(1), pp. 53-61 (2001).

31. Sveningsson, A. and Davidson, L. "Assessment of realizability constraints in $\overline{v^2} - f$ turbulence models", *J. Heat and Fluid Flow*, **25**(5), pp. 785-794 (2004).

32. Heschl, C.H., Sanz, W. and Klanatsky, P. "Implementation and comparison of different turbulence models for three dimensional wall jets with FLUENT", *CFD Forum 2005*, Bad Nauheim, Deutschland (2005).

33. Liuboja, M. and Rodi, W. "Calculation of turbulent wall jets with an algebraic Reynolds stress model", *ASME Journal of Fluid Engineering*, **102**(4), pp. 350-356 (1980).

34. Launder, B.E. and Rodi, W. "The turbulence wall jet- measurement and modeling", in *Annual Review of Fluid Mechanic*, **15** (1983).

35. Choi. S. and Garcia. H. "$k - \varepsilon$ turbulence modeling of density currents developing two dimensionally on a slope", *Journal of Hydraulic Engineering*, **128**(1), pp 55-63 (2002).

36. Parneix, S., Durbin, P. and Behnia, M. "Computation of 3-D turbulent boundary layer using the $\overline{\nu^2} - f$ model", *Flow, Turbulence and Combustion*, **60**(1), pp. 19-46 (1998).

37. Launder, B.E. and Sharma, B. "Application of energy-dissipation model of turbulence to the calculation; A spinning disk", *Letter in Heat and Mass Transfer*, **1**, pp. 131-138 (1974).

38. Durbin, P.A. "Separated flow computations with $k - \varepsilon - \overline{v^2}$ model", *AIAA J.*, **33**(4), pp 659-664 (1995).

39. Durbin, P.A. and Pettersson, B.A., *Statistical Theory and Modeling for Turbulent Flow*, John Wiley & Sons LTD, Chapter II, pp. 109-131 (2001).

40. Durbin, P. "On the $k - \varepsilon$ stagnation point anomaly", *Int. J. Heat and Fluid Flow*, **17**(1), pp. 89-90 (1996).

41. Manceau, R., Wang, M. and Laurence, D. "Inhomogeneity and isotropy effects on the redistribution term in Reynolds-averaged Navier-Stokes modeling", *J. of Fluid Mechanics*, **438**, pp. 307-338 (2001).

42. Behnia, M., Parneix, S., Shabany, Y. and Durbin, P.A. "Numerical study of turbulent heat transfer in confined and unconfined impinging jets", *International Journal of Heat and Fluid Flow*, **20**(1), pp. 1-9 (1999).

43. Akiyama, J., Ura, M. and Wang, W. "Physical-based numerical model of inclined starting plumes", *J. Hydraulic Eng., ASCE*, **120**(1), pp. 1139-1157 (1994).

44. Ferziger, J.H. and Peric, M., *Computational Methods for Fluid Dynamics*, Springer, Berlin, Germany (1996).

45. Rhie, C.M. and Chow, W.L. "Numerical study of the turbulent flow past on airfoil with trailing edge separation", *J. AIAA*, **21**(11), pp. 1527-1532 (1983).